RAA 2021 Vol. **21** No. **6**, 148(10pp) doi:10.1088/1674-4527/21/6/148

http://www.raa-journal.org *http://iopscience.iop.org/raa*

***R**esearch in*
***A**stronomy and*
***A**strophysics*

Evolvement of microwave spike bursts in a solar flare on 2006 December 13

Jian-Fei Tang[1,2,3], De-Jin Wu[2], Jun-Lin Wan[1,4], Ling Chen[2] and Cheng-Ming Tan[3]

[1] Xinjiang Astronomical Observatory, Chinese Academy of Sciences, Urumqi 830011, China; *jftang@xao.ac.cn*
[2] Key Laboratory of Planetary Sciences, Purple Mountain Observatory, Nanjing 210023, China
[3] CAS Key Laboratory of Solar Activity, National Astronomical Observatories, CAS, Beijing 100101, China
[4] School of Astronomy and Space Science, University of Chinese Academy of Sciences, Beijing 100049, China

Received 2020 November 19; accepted 2021 January 29

Abstract Solar radio spikes are one of the most intriguing spectral types of radio bursts. Their very short lifetimes, small source size and super-high brightness temperature indicate that they should be involved in some strong energy release, particle acceleration and coherent emission processes closely related to solar flares. In particular, for the microwave spike bursts, their source regions are much close to the related flaring source region which may provide the fundamental information of the flaring process. In this work, we identify more than 600 millisecond microwave spikes which recorded by the Solar Broadband Radio Spectrometer in Huairou (SBRS/Huairou) during an X3.4 solar flare on 2006 December 13 and present a statistical analysis about their parametric evolution characteristic. We find that the spikes have nearly the same probability of positive and negative frequency drifting rates not only in the flare rising phase, but also in the peak and decay phases. So we suppose that the microwave spike bursts should be generated by shock-accelerated energetic electrons, just like the terminational shock (TS) wave produced by the reconnection outflows near the loop top. The spike bursts occurred around the peak phase have the highest central frequency and obviously weak emission intensity, which imply that their source region should have the lowest position with higher plasma density due to the weakened magnetic reconnection and the relaxation of TS during the peak phase. The right-handed polarization of the most spike bursts may be due to the TS lying on the top region of some very asymmetrical flare loops.

Key words: Sun: activity — Sun: flares — Sun: radio radiation

1 INTRODUCTION

Solar radio spike bursts are one type of spectral fine structures (FSs) associated with solar flares. It has undergone for nearly 60 years since the first detection of solar radio spike bursts at meter wavelengths (Elgarøy 1961). In subsequent years, spikes were observed not only in the decametric wavelengths (Barrow & Saunders 1972) but also detected at decimetric wavelengths (Benz 1985, 1986) and microwave wavelengths (Droege 1977; Slottje 1978; Staehli & Magun 1986; Benz et al. 1992). Due to the spike bursts demonstrating the shortest time scales at about several milliseconds (Staehli & Magun 1986), the narrowest frequency bandwidth on the order of about 1% (Benz 1985) and the very high brightness temperatures (up to and even exceed 10^{15} K) (Benz 1985, 1986), it has attracted the extensively attention of many researchers.

Many people presented the investigations from observations and theoretical models. For the duration of single spikes, it is about $50 \sim 100$ ms around 250 MHz, $10 \sim 50$ ms around 460 MHz and $3 \sim 7$ ms around 1420 MHz (Benz et al. 1982). Guedel & Benz (1990) present a detailed study of the temporal properties of single spikes and showed a negative correlation of the averaged duration of spike bursts with the frequency as $\tau \propto f^{-1.34\pm0.14}$ at frequencies between $\sim$ 300–1000 MHz. Sirenko & Fleishman (2009) investigated the dependence of the durations of millisecond radio spikes on emission frequency and refined the Güdel-Benz law (Guedel & Benz 1990) as $\tau \propto f^{-1.29\pm0.08}$. The relative bandwidths of the spike bursts are on the order of about 1% (Benz 1985; Staehli & Magun 1986). The average relative bandwidths of individual spikes are 1.3% and 4.1% for two clusters of spikes recorded in 1.08–1.6 GHz and 1.0–1.35 GHz, as is analyzed by Csillaghy & Benz (1993). They also studied the relations between the bandwidth with other observed parameters and pointed

out that there is no clear relationship between the bandwidth and central frequency, and the bandwidth vary significantly from one to another event. Csillaghy & Benz (1993) claimed that it is the source inhomogeneity which form the observed bandwidth rather than the emission process. Messmer & Benz (2000) found that the minimum relative bandwidth of individual spike for two considered events are 0.17% and 0.41%. They proposed that the minimum relative bandwidth may be formed by the natural bandwidth of the emission process, and the broader spikes are due to the source inhomogeneity. Spike bursts usually have strong circular polarization (Slottje 1978), and it can vary from 0 to 100% (Benz et al. 1982; Staehli & Magun 1986).

According to the relative frequency bandwidth and the characteristic scale of corona plasma parameter, the linear size of the sources of individual spikes are smaller than 200 km (Benz 1986; Bastian et al. 1998; Fleishman & Mel'nikov 1998). Correspondingly, for a circular source, the brightness temperature of the radio spike bursts is up to 10^{15} K (Benz 1985, 1986), this means that radio spikes must be produced by some coherent emission mechanisms. Theoretical models of solar radio spike bursts include the plasma emission (Kuijpers et al. 1981; Tajima et al. 1990; Wentzel 1991; Bárta & Karlický 2001) which involve the nonlinear wave-wave coupling process and the electron cyclotron maser emission (ECME) (Melrose & Dulk 1982; Sharma & Vlahos 1984; Winglee et al. 1988; Aschwanden 1990; Fleishman & Yastrebov 1994; Fleishman & Mel'nikov 1998; Fleishman et al. 2003). The latter is the most favored emission process for radio spikes. Fleishman & Melnikov (1999) made a detailed comparison between the spike properties and predictions of various theoretical models, and pointed out that ECME could explain almost all observational characteristics. Fleishman & Arzner (2000) pointed out that the quasi-linear saturation of ECME can account for the time profiles of spikes with a Gaussian rise phase and an exponential decay phase. Rozhansky et al. (2008) made a detailed statistical analysis about the parameters distribution of the radio spikes and found that the theoretical model based on the ECME mechanism agrees excellently with the observed distribution of the relative bandwidth. Fleishman et al. (2003) proposed that the source of spike cluster is a loop filled with fast electrons which have the loss-cone anisotropy distribution. The individual spikes are generated in a local source inside the loop when the local anisotropy is increased in comparison with the averaged one to produce the ECME mechanism. Although much progress has been made in observations and theory for the millisecond radio spikes, the evolution of spikes observation parameters with flare process is still rarely discussed. Radio spike bursts are deemed the prompt signal of energetic particles accelerated by magnetic reconnection or shock wave during the flare. In particular, in the microwave frequency range, the source regions of spike bursts are believed to be much close to the flaring source region and may provide much more information on the primary energy releasing and particle acceleration, and such information may help us to judge the different physical pictures of the solar flares, such as described in the standard flare models (Shibata et al. 1995; Lin & Forbes 2000) and the recent proposed model (Tan et al. 2020), etc. It is significative to investigate their evolutional properties of the observational parameters for understanding the flare energy release, the acceleration and propagation of particles.

On 2006 December 13, an X3.4 flare with a fast halo coronal mass ejection (CME) was observed in active region NOAA10930. A great number of radio spikes were detected at the frequency range 2.60-3.80 GHz by SBRS/Huairou. Wang et al. (2008) analyzed the observed characteristics of 19 clusters of spikes and divided them into five classes based on their polarization or relationship with other radio bursts. According to the soft X-ray flux intensity observed by the Geostationary Operational Environmental Satellite (GOES), we divide the whole flaring process into the rising, peak, and decay phases. We investigate the temporal evolution of the observational parameters of spike bursts, including central frequency, flux density, and polarization degree, and frequency drifting rates in different phase of the flare. The results show that the individual spikes have the extremely observational characteristics which should be associated with some coherent radiation processes. Since the nearly equal probability of negative and positive frequency drifting rates of the spike bursts, we propose that the energetic electrons associated with the radio spike bursts are accelerated by shock waves, such as the termination shock (TS) wave. The super-magnetosonic reconnection outflows impinge on the closed magnetic loops and produce the TS near the looptop. The decrease of the magnetic reconnection rate leads to the relaxation of the termination shock during the peak phase, which is the reason that the spike bursts in the peak phase have the highest center frequency and the obviously weak emission intensity. The polarization of spike bursts is determined by the position of TS wave on the magnetic loops. This paper is organized as follows: Section 2 introduces the observation data and presents the main features of spikes. Theoretical analysis and discussions of the evolutional properties are described in Section 3. Finally, conclusions are provided in Section 4.

2 OBSERVATIONAL PROPERTIES

2.1 Instrument

The SBRS/Huairou is a broad bandwidth microwave spectrometer. Its remarkable characteristics are the high cadence, high frequency resolution, high sensitivity and the wide frequency coverage. The SBRS/Huairou is constituted of three parts: 1.10–2.06 GHz, 2.60–3.80 GHz, and 5.20–7.60 GHz (Fu et al. 1995, 2004; Yan et al. 2002). However, only the 2.6–3.8 GHz spectrometer was operating well around the X3.4 flare/CME event on 2006 December 13. In the frequency range of 2.60–3.80 GHz, there are four filter-bands and 30 channels in each filter-band. The frequency resolution, i.e. the frequency width of each channel is 10 MHz. Because it needs 2 ms for data sampling of 30 channels, the temporal resolution for the frequency band of 1.2 GHz is 8 ms. In order to identify the weak solar burst structures, the wavelet methods have been adopted for data processing. The calibration method for the observation data was put forward by Tanaka et al. (1973). The standard flux density values of the quiet Sun are calculated from the daily flux values published by Solar Geophysical Data (SGD) at frequencies: 15400, 8800, 4995, 2800, 2695, 1415, 610, 410, and 245 MHz (Fu et al. 2004). The receiver will use the nonlinear calibration method instead of linear method when the bursts are very strong (Yan et al. 2002).

2.2 Observation

AR 10930 is an isolated active region near the east limb of the solar disk. According to SGD information, it was a β region with a large leading sunspot on 2006 December 6 and developed into a $\beta\gamma\delta$ region on December 7 (Zhang et al. 2008). There was a significant flux emergence in the following sunspot before the major event on December 13. The following sunspot moved eastward rapidly and rotated counterclockwise around its center up to 240° before the major flare (Zhang et al. 2007). On December 13, a powerful flare event took place. This flare event is classified as X3.4 from soft X-ray emission observed by GOES satellite. Figure 1 plots the entire flare process with the GOES SXR at $1-8$ Å, $0.5-4$ Å and the microwave emission at 3.67 GHz. The top panel shows that the SXR event started at 02:14 UT, reached to the maximum at 02:40 UT and followed by a nearly 2 hour decay phase. The radio bursts started at 02:20 UT and lasted after 04:50 UT accompanied with many kinds of spectral fine structures, such as spikes, zebra patterns, fibers, quasi-periodic pulsations, microwave type III bursts and patches. This flare/CME event has been comprehensively studied from different points of view (Kosovichev & Sekii 2007; Tan et al. 2007; Zhang et al. 2007; Ning 2008; Tan 2008; Guo et al. 2008; Zhang et al. 2008; Wang et al. 2008; Minoshima et al. 2009; Tan et al. 2010). In order to investigate the evolution of radio spikes during the flaring process, we plotted the whole flaring process into three phases from the soft X-ray flux intensity, the rising phase (with positive flux derivative, 02:14 UT-02:35 UT, lasted for 15 minutes), the peak phase (the flux derivative is nearly around 0, 02:35 UT-02:45 UT, lasted for 10 minutes), and the decay phase (with negative flux derivative, after 02:45 UT, lasted for more that 2 hours), see Figure 1.

In order to obtain a reasonable statistic investigation of the microwave spike bursts, we assume that the selection criteria of individual spike bursts are the duration more than 8 ms but less than 50 ms (Wang et al. 2008), the frequency bandwidth less than 150 MHz. With the above limitations, we obtained more than 600 microwave spikes during the flare event. Figure 2 presents a group of spikes appeared during 02:28:58 – 02:29:10 UT in the rising phase. The spikes usually have complex structures and always associated with other spectral fine structures. Figure 2 shows that the spikes of rising phase are accompanied with a bright patch. With the high temporal and frequency resolutions (8 ms and 10 MHz) of SBRS/Huairou, we can identify and confirm the existence of spikes clearly and pick up their parameters easily by scrutinizing the dynamic spectrograms. These parameters include the central emission frequencies (f_0), frequency bandwidth (Δf), duration (D), flux density (S_R), polarization degree (PD), and frequency drifting rate (FDR) of each individual spike.

1. Duration (D)

As mentioned above, solar microwave spike bursts have the shortest time scales among all the known types of solar radio bursts. Observations show the time profiles of spikes always compose of a Gaussian rise phase and an exponential decay phase (Guedel & Benz 1990; Fleishman & Mel'nikov 1998). We may define the duration of a single spike as the time interval between the rising phase and the decaying phase of the spike at half maximum flux. Figure 3 presents the distribution of duration of the individual radio spikes, where the horizontal coordinates are the central frequencies of the spikes. It shows that the duration of individual spikes ranges from 16 ms to 48 ms and the amount of spikes decreases with its duration.

2. Emission frequency (f, f_1, f_2)

As for microwave spike bursts, the parameters of emission frequencies include their starting frequency (f_1), ending frequency (f_2), and the central frequency ($f = \frac{1}{2}(f_1 + f_2)$). According to the code programmed by

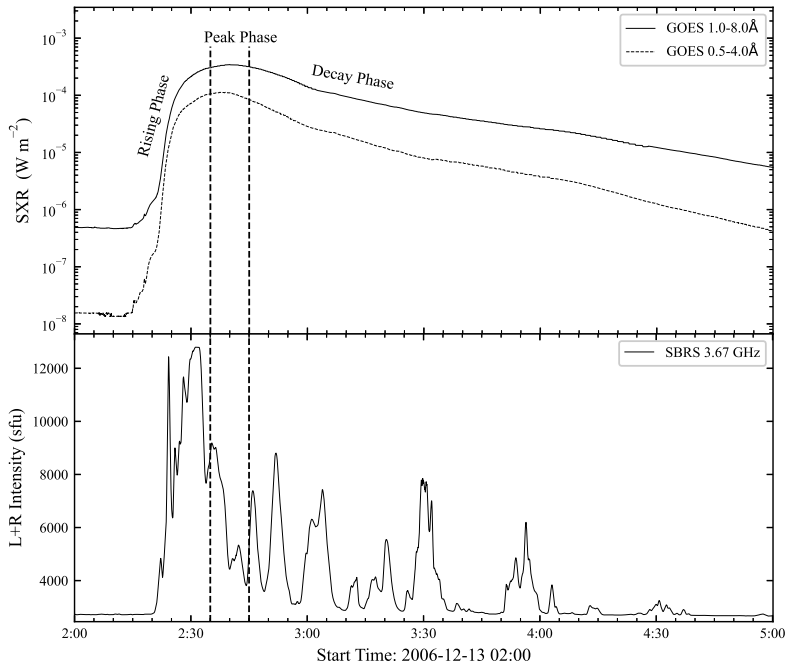

Fig. 1 The profile of soft X-ray at $0.5 \sim 4.0$ Å, $1 \sim 8$ Å (*GOES8*) and microwave emission at 3.67 GHz of the event on 2006 December 13.

Yan et al. (2002), we can distinguish the spike events which superposed on the radio continuum and identify the frequency range of each spike clearly. From Figure 3, one can find that the central frequencies of spikes in the rising phase rang between 2.6 GHz and 3.4 GHz. In the peak phase, however, the central frequencies range from 3.0 GHz to 3.8 GHz. The central frequencies of individual spikes in decay phase overspread the whole observing frequency range of the spectrometer.

3. Bandwidth (Δf)

Csillaghy & Benz (1993) pointed out that the bandwidth of spike bursts should be formed mainly by the inhomogeneity in source region, rather than being a natural bandwidth of the underlying emission process. Furthermore, Messmer & Benz (2000) claimed that the minimum relative bandwidth of spike bursts should be formed by the natural bandwidth of the emission process, while the broader spikes are due to their source inhomogeneity. So, the bandwidth and its distribution may reflect the details of the spatial structure of the source region. The bandwidth is defined as the difference between the starting frequency to the ending frequency. In this work, we define the (half-power) bandwidth (Δf) at practically instantaneous time of the peak flux. In order to compare in different frequency range, the relative bandwidth is much more meaningful which is defined as $\Delta f/f \times 100\%$. The evolution of the relative bandwidth of spikes from the flare rising phase via peak phase to decay phase is shown in Figure 4. Similar to Figure 3, the horizontal coordinates are the central frequencies of spikes. From Figure 4 one can find that most spike bursts have the relative bandwidth range between $0.5\%-3\%$. The average relative bandwidth of spike bursts is around 1.5%, which decreases slightly with the evolution of flare.

4. Flux density (S_R)

The flux density of individual spike burst is defined as $S = I - I_0$. Here, I and I_0 are the detected flux intensity and the background emission flux intensity, respectively. Almost all the spikes in this work are right-handed polarization and parameter $S_R = I_R - I_{R0}$ represents the flux density of spike. Figure 5 presents the flux density of individual spikes in the different phases. From Figure 5 one can find that the great mass of spikes in the rising and decay phase have the flux density larger than 100 sfu, but the flux density of most spikes in the peak phase less than 100 sfu, that is to say, the emission intensity of the spikes during peak phase is obviously weaker than that during the rising and decay phases.

5. Polarization degree (PD)

The polarization degree of spike burst is defined as $PD = \frac{S_R - S_L}{S_R + S_L} \times 100\%$, where $S_R = I_R - I_{R0}$ and $S_L = I_L - I_{L0}$ indicate the flux intensities of right-handed circular polarization and left-handed circular polarization, respectively. I_R (I_L) is the recorded flux intensity and I_{R0}

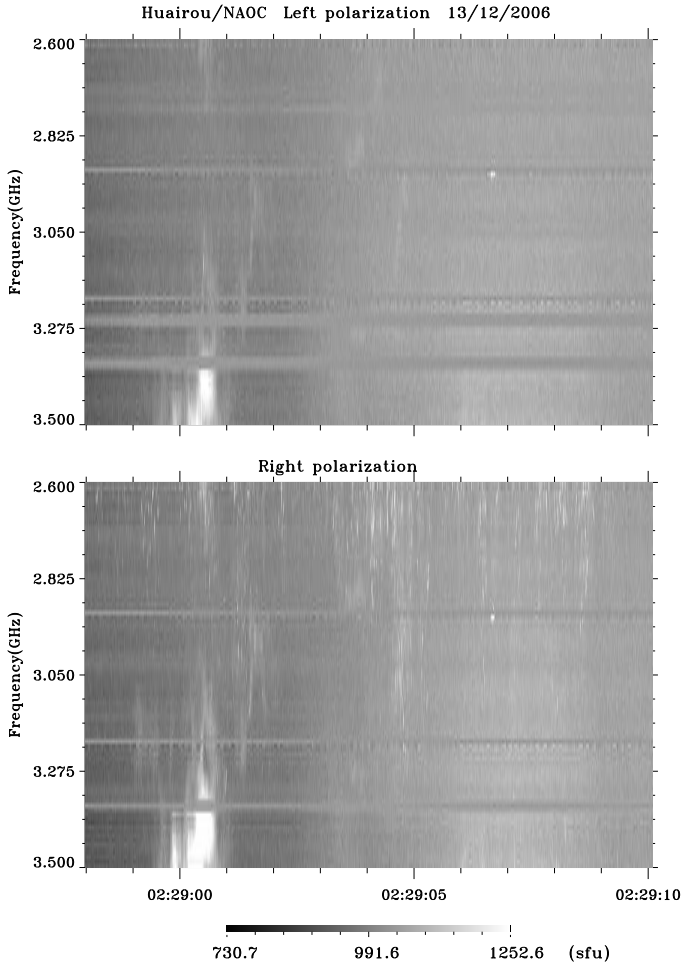

Fig. 2 An example of solar microwave spike group occurred in the rising phase. The spikes are accompanied with a bright patch and display a strong right-handed polarization.

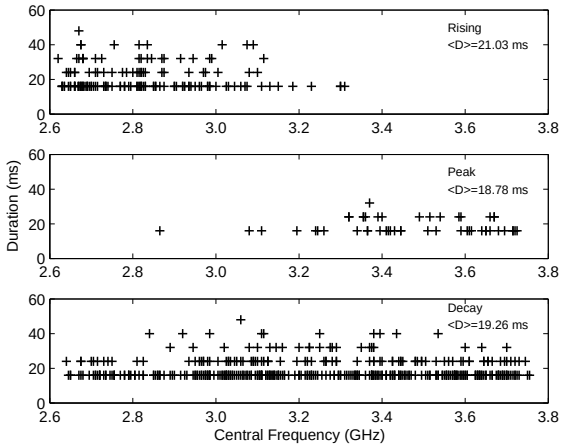

Fig. 3 Distribution of duration of the individual spikes vs. central frequency in different phases of the flare.

(I_{L0}) is the background flux intensity (Aschwanden 1986). If the right-handed circular polarization is dominated, $PD > 0$, conversely, when the left-handed circular polarization is dominated, $PD < 0$. When $\mid PD \mid > 55\%$, it means strongly polarized; when $\mid PD \mid = 15 \sim 55\%$, it means mildly polarized; and when $\mid PD \mid < 15\%$, it is regarded as weakly polarized.

6. Relative frequency drifting rate

Frequency drift is one of the main characteristics of solar radio spike bursts which directly reflects the dynamic information of the emission excitor. It is defined as the temporal variation of the frequency, i.e., df/dt. The relative frequency drift is df/fdt. Figure 6 is the distribution of the relative frequency drift of individual spikes vs. the central frequency in different phases of the flare. From Figure 6 one can find that the spike bursts have nearly same probability of negative and positive frequency drifting rates during the whole flare. This indicate that the

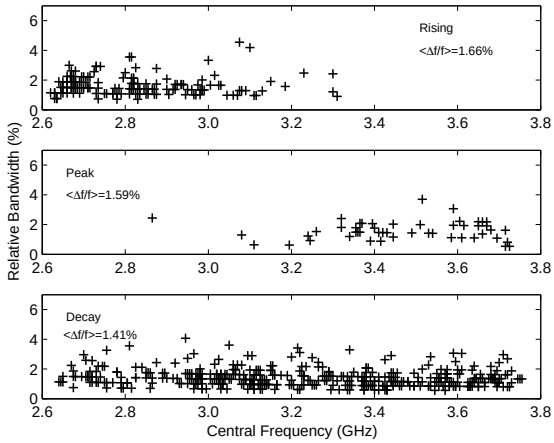

Fig. 4 Distribution of relative bandwidth of the individual spikes vs. central frequency during different phases of the flare.

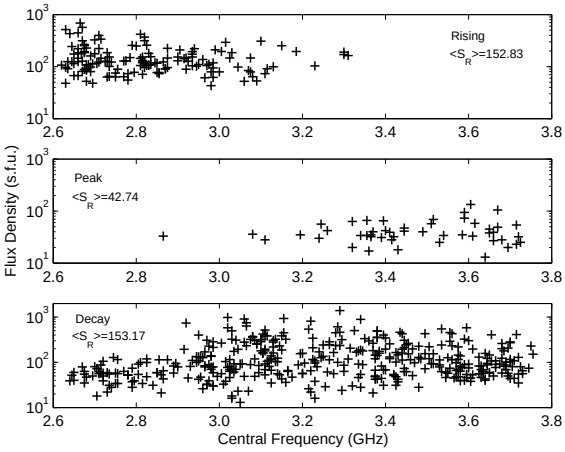

Fig. 5 Distribution of flux density of the individual spikes vs. central frequency during the different phases of the flare.

energetic electrons producing the spikes are equally likely to move up and down.

7. Occurrence rate

The occurrence rate of microwave spike bursts is defined as the number of spikes per minute in the whole observed frequency band.

We list the ranges and averaged values of the observational parameters in different phases of the flare in Table 1. Here, in the first column, AV, AAE, and ARE are the average value, average absolute error, and the average relative error of the observational parameters, respectively. For the duration and frequency bandwidth, the absolute errors directly depend on the temporal and frequency resolutions, i.e., 8 ms and 10 MHz. The absolute errors of the other observational parameters are caused by the uncertainties of the measured duration, frequency, and

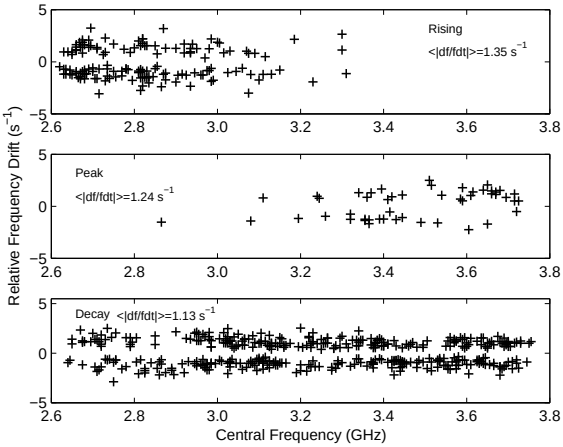

Fig. 6 The distribution of the relative frequency drift rate of spikes vs. central frequency during the different phases of the flare.

intensity. The second and third columns are the number of the spike bursts per minute and the duration of individual spike. The fourth, fifth and sixth columns are the central frequency, bandwidth and relative bandwidth, respectively. The seventh column is the flux density and the eighth column is the polarization degree, the last column is the magnitude of the relative frequency drift rate. With the selection criteria of duration and bandwidth, more than 600 radio spikes have been detected, including 148 spikes in the rising phase, 49 spikes in the peak phase, and 405 spikes in the decay phase. From Table 1 one may find that the occurrence rate decreases from 9.9 spikes per minute in the rising phase, via 4.9 spikes per minute in the peak phase to 3.2 spikes per minute in the decay phase. The duration of individual spike ranges from 16 ms to 48 ms, with the minimum averaged duration of about 18.78 ms occurred in the peak phase. The central frequency of individual spike in the rising, peak, and decay phases are 2585–3310 MHz, 2865–3725 MHz, and 2640–3755 MHz, respectively. Radio spikes have the highest averaged mean central frequency of 3467.86 MHz and maximum averaged bandwidth of 55.31 MHz during the peak phase. The flux density of individual spike in the three phases are 43–688 sfu, 13–134 sfu, and 13–1397 sfu, respectively. The averaged flux density in the peak phase is only about 1/3 of that in the rising and decay phases. Table 1 also shows that the spikes in peak phase have the minimum mean polarization degree.

3 ANALYSIS AND DISCUSSIONS

Solar radio spikes usually appear in groups of pulses on the dynamic spectrum with short-duration and narrow-band. Benz (1985) initially interpreted a single spike as a microflare, and the large number of spikes in flares as

Table 1 Parameters of Radio Spikes of Three Flare Phases

Phase	SO (min^{-1})	D (ms)	f (MHz)	Δf (MHz)	Δf/f (%)	S_R (sfu)	PD (%)	$\lvert df/fdt\rvert$ (s^{-1})
Rising	9.9	16–48	2585–3310	20–140	0.71–4.55	43–688	39.13–100	0.31–3.33
AV	-	21.03	2828.37	47.03	1.66	152.83	87.41	1.35
AAE	-	8	128.67	10	0.50	70.72	10.18	0.46
ARE	-	38.04%	4.55%	21.26%	30.12%	46.27%	11.65%	34.07%
Peak	4.9	16–32	2865–3725	20–130	0.54–3.70	13–134	38.77–100	0.50–2.70
AV	-	18.78	3467.86	55.31	1.59	42.74	78.26	1.24
AAE	-	8	155.16	10	0.49	16.08	19.78	0.38
ARE	-	42.60%	4.47%	18.08%	30.82%	37.62%	25.27%	30.64%
Decay	3.24	16–48	2640–3755	20–120	0.56–4.08	13–1397	26.83–100	0.34–2.82
AV	-	19.26	3242.84	45.53	1.41	153.17	90.00	1.13
AAE	-	8	259.03	10	0.44	111.59	8.90	0.34
ARE	-	41.54%	7.99%	21.96%	31.21%	72.85%	9.89%	30.09%

SO is the occurrence rate of spike, D is the duration, f is the central frequency, Δf and Δf/f are the bandwidth and relative bandwidth, respectively. S_R is the flux density, PD is the degree of polarization, $|df/fdt|$ is the magnitude of the relative frequency drift rate. AV is the average value of the parameters, AAE and ARE denote the average absolute errors and average relative errors, respectively.

a signature of highly fragmented energy release. Other models are proposed to interpret the formation of clusters of radio spikes. The model proposed by Fleishman et al. (2003) considers the clusters as a result of strong local inhomogeneities, which form local traps and may give rise to the wave amplification process. An alternate model proposed that solar small-scale microwave bursts are produced by energetic electrons accelerated from the magnetic reconnection in the small-scale magnetic islands, which is caused by the tearing-mode instability of the electron beam moving along the flaring plasma loops (Tan 2010; Tan & Tan 2012; Tan 2013). From Figure 6 one can find that both the negative and positive frequency drifting spikes are detected. The frequency drift rate and occurrence probability of the positive and negative drift spikes are nearly equivalent in different phases of the flare. Additionally, observations also indicated that almost all the radio spikes had a strong right-handed polarization (Wang et al. 2008). Therefore, we suggest that the related energetic electrons should be accelerated by some shock waves, such as the flare terminational shock (TS), produced by reconnection outflows or downward energetic electron beams impinge upon the flaring loop top (Chen et al. 2015; Tan et al. 2019). The 3D magnetic field configuration of the flare on 2006 December 13 consists of two parts, a highly sheared, twisted core field and a less sheared envelop field straddling over the core field (Guo et al. 2008; Li et al. 2009). Guo et al. (2008) claimed the standard tether-cutting model for this eruptive event: the core field lines will reconnect before the major event take place because of the sunspot rotation and/or emerging flux; then magnetic reconnection occurs between envelop field lines when the closed arcade envelope field is opened and stretched out. Zhang et al. (2007) examined the evolution of magnetic field and sunspot in the active region and found that the smaller sunspot rotates up to 200° before the major event takes place. Wang et al. (2008) found that the location of SOT brightening located in one of the flare ribbons near the larger sunspot could be the sources of the spikes with left-handed polarization. Based on these observational studies of magnetic fields and sunspots, we proposed that the physical picture of the radio sources is as follows: the small-scale magnetic reconnection occurs between the core field lines due to the sunspot rotation and/or emerging flux before the major event. Then the envelope field will be opened and stretched out, magnetic reconnection between envelope field lines occur. Flaring magnetic reconnection accelerates electrons and produces the upward and downward nonthermal electron beams, which generate the normal and reverse-sloped type III bursts, respectively. Meanwhile, the super-magnetosonic downward nonthermal electron beams will produce a TS at the relatively dense flare loop top. Energetic electrons accelerated by the TS are the source of the detected radio spike bursts, which demonstrate a random distribution of negative and positive frequency drifting during the whole flare.

The observed bandwidth constrains the possible sources sizes of the radio spikes. Assuming that the emission frequency depends on a characteristic frequency (the gyrofrequency or the local plasma frequency), the upper limit of sizes of individual spikes sources could be estimated by (Benz 1986):

$$l = \lambda \frac{\Delta f}{f}, \tag{1}$$

where λ is the scale length corresponding to the characteristic frequency, $\Delta f/f$ is the relative bandwidth. Taking $\lambda = 10^4$ km as Benz (1985) done, the mean space scale of individual spikes in different flare phase are 166km, 159km and 141km, respectively. According to the flux density and the space scale of spikes, the brightness

temperature of individual spikes can be derived from:

$$l(\mathrm{km}) = 9.64 \times 10^7 \left(\frac{S(\mathrm{sfu})}{T_b(\mathrm{K})} \right)^{1/2}, \qquad (2)$$

where l and S are the source size and the flux density of spikes, respectively. With the mean space scale and the mean flux density, the mean brightness temperatures of spikes are 5.15×10^{13} K, 1.57×10^{13} K, and 6.59×10^{13} K in the rising, peak, and decay phase, respectively. From Table 1, one can find that the spikes have a short duration (tens of ms) and a strong polarization degree. As summarized by Melrose & Dulk (1982), the radio spikes bursts with such a small source size, high brightness temperature, short lifetime, and strong polarization degree unambiguously suggest a coherent emission mechanism, electron cyclotron maser emission.

From Table 1, one can find that the spikes of peak phase have the shortest mean duration and the highest mean central frequency. According to the characteristic frequency of radio emission (i.e., the gyrofrequency or the plasma frequency), which is determined by the background plasma density or magnetic field strength, a high central frequency indicates a low and dense source position. After the magnetic reconnection of the envelop field begins, the reconnection outflows hits the top of the flare loop and produces TS wave. The TS front, where the spikes associated electrons were accelerated, moves downwards as the recurring hits of downwards outflows. From Figure 1 one can find that the microwave emission has a local minimum value during the peak phase. Li et al. (2009) investigated the magnetic reconnection rate and found it is temporally well-correlated with the microwave emission. That is, during the peak phase, the magnetic reconnection of the envelop field becomes weaker. Therefore, the TS front should have the lowest position in the peak phase because of its relaxation process. Due to the lowest position and the extrusion of TS wave, the emission sources of the spike bursts in the peak phase should have the strongest magnetic field and the highest density. This is why they have the highest mean central frequency. The short duration of the spikes in the peak phase may be related to the high density in the source region. The wave-wave and wave-particle interactions are more likely to occur in the high-density plasma, therefore, the growth rate of the waves involved in the spikes emission can be damped even more (Casillas-Pérez et al. 2019). Table 1 also shows that the occurrence rate of microwave spike bursts decreases with flare evolution. The rising phase has the strongest magnetic reconnection of the envelop field and produces the strongest TS wave. In the decay phase, although magnetic reconnection often occurs and the TS wave should stronger than that in the peak phase, however, the decay phase lasts for a long time.

Figure 5 and Table 1 show that the flux density of individual spikes in the peak phase is much lower than that in the rising and decay phases. We suggest that the radio spikes should be produced by the ECM mechanism, it can be amplified effectively if the frequency ratio of gyrofrequency to plasma frequency is large enough ($\omega_{ce}/\omega_{pe} \gtrsim 1$). The growth rate of maser instability is mode dependent (the $X-$mode has larger growth rate than $O-$mode) and is proportional to n_b/n_0, here n_b and n_0 are the number densities of the energetic and thermal electrons component, respectively. As discussed above, the spike bursts during the peak phase have the densest sources, i.e., the largest n_0. On the other hand, the magnetic reconnection of the envelop field during the peak phase becomes weaker, so the TS generated by the reconnection outflows also becomes weaker, and the spike-associated energetic electrons accelerated by the TS becomes fewer and less energetic. Therefore, the lower energy and fewer number energetic electrons and the highest density of background thermal plasma lead to the minimum growth rate of ECME. This may be the main reason why the emission intensity of the spike bursts during peak phase is obviously weaker than that during the rising and decay phases.

Table 1 shows that the spikes in the peak phase have the minimum value of mean polarization degree. Wang et al. (2008) showed that almost all the spike bursts have a right-handed polarization except a group of spikes in the peak phase. The polarization characteristic of spike bursts is closely related to the magnetic configurations of the source region. Imaging observations (Ca II H) of Hinode/SOT and HXR observations from RHESSI show that the related flare has a typical two-ribbon. It is structured between a big leading sunspot and a smaller following sunspot. The 3D magnetic field configuration associated with this flare derived by nonlinear force-free field extrapolation consists of a highly sheared core field and a less sheared envelop arch field (Guo et al. 2008). The envelop field rooted on the concentrated polarity (the following sunspot) and connected to the dispersive leading sunspot (Guo et al. 2008). The major flare was triggered after the following sunspot rotated up to 200° and the reconnection of envelop field begin. Then the TS was produced near the top of flare loop by the downward outflows and accelerated energetic electrons which responsible for the spike bursts. Observations from Hinode/SOT also show that the two ribbons of the flare are very asymmetrical Jing et al. (2008); Wang et al. (2008); Li et al. (2009); Tan et al. (2010). Therefore, we may suggest that the envelop field rooted on these two ribbons is also asymmetrical and the vertices are skewed to the side of the short ribbon which associated with

the concentrated positive polarity. During the peak phase, some uncertainties may reduce the asymmetry of the envelop field. This is why the spike bursts in the peak phase have relatively weak averaged polarization and almost all the spike bursts have a right-handed polarization.

4 CONCLUSIONS

Millisecond radio spikes are one of the most intriguing spectral types of solar radio emission. Since its first detection about half century ago, it has attracted a lot of theorists' attention because of its extremely short characteristic time scales, very narrow spectral widths, and super-high brightness temperature. In this work, we make a statistical analysis of the observational parameters of the microwave spikes and their temporal evolution in a flare on 2006 December 13. We found that the microwave spikes occurred in the flaring rising phase, as well as in the peak and decay phases. They have many unique evolutionary features.

(1) Although most microwave spikes occurred in the decay phase, but the occurrence rate is still decreasing from the rising phase via peak phase to decay phase. This is reasonable to imply that the energy release is much stronger in the rising phase than that in the peak and decay phases.

(2) The microwave spikes are characterized by very short duration, narrow frequency bandwidth, small spatial scale, super-high brightness temperature, and a strong polarization degree. Their brightness temperature exceed 10^{13} K which indicate that they are generated by some strong coherent emission processes.

(3) Both the negative and positive frequency drifting spikes are detected with nearly equal probability in the rising phase as well as in the peak and decay phase of the flare event. Therefore we suggest that some shock waves may contribute to the particle accelerations, and the energetic electrons associated with the microwave spikes are possibly accelerated by TS waves producing by the outflows of magnetic reconnection near the flaring looptop.

(4) During the peak phase, due to the magnetic reconnection is weakened and the relaxation of TS wave, the microwave spikes produced by the TS-accelerated electrons have the lowest and densest source. This may be the reason why the microwave spikes in the peak phase have the highest mean central frequency.

(5) The microwave spikes in flare peak phase have the minimum average duration. The minimum average duration implies a short time of energetic electrons pass through the source region due to the high density in the source region. Because the wave-wave and wave-particle interactions are more likely to occur in the high-density plasma. The average flux density of microwave spikes in the rising and decay phase is much higher than that in the peak phase. The minimum growth rate of ECM instability may account for the minimum flux density in the peak phase.

(6) The asymmetry of the envelop field (flare loop) rooted on the asymmetrical ribbons may be the reason why almost all the spike bursts are right-handed polarization.

The above evolutionary features of microwave spikes may provide meaningful information to limit the theoretical models of solar eruptions. However, it is still not comprehensive for no imaging observations at the corresponding frequencies. Next step, we plan to collect the spectral-imaging observations to demonstrate the position and spatial configurations of the microwave spikes, the observations may come from MUSER (Yan et al. 2009) and other international solar spectral radioheliographs.

Acknowledgements This work is supported by 2018-XBQNXZ-A-009 and 2017-XBQNXZ-A-007, by the National Natural Science Foundation of China (Grant Nos. 11673055, 41531071, 11873018, 11773061, 11790301 and 11973057), and the Tianshan Youth funding (Grant 2017Q401), and by Key Laboratory of Solar Activity at National Astronomical Observatories, CAS.

References

Aschwanden, M. J. 1986, Sol. Phys., 104, 57
Aschwanden, M. J. 1990, A&A, 237, 512
Barrow, C. H., & Saunders, H. 1972, Astrophys. Lett., 12, 211
Bárta, M., & Karlický, M. 2001, A&A, 379, 1045
Bastian, T. S., Benz, A. O., & Gary, D. E. 1998, ARA&A, 36, 131
Benz, A. O. 1985, Sol. Phys., 96, 357
Benz, A. O. 1986, Sol. Phys., 104, 99
Benz, A. O., Jaeggi, M., & Zlobec, P. 1982, A&A, 109, 305
Benz, A. O., Su, H., Magun, A., & Stehling, W. 1992, A&AS, 93, 539
Casillas-Pérez, G. A., Jeyakumar, S., Carrillo-Vargas, A., & Pérez-Enríquez, H. R. 2019, Sol. Phys., 294, 10
Chen, B., Bastian, T. S., Shen, C., et al. 2015, Science, 350, 1238
Csillaghy, A., & Benz, A. O. 1993, A&A, 274, 487
Droege, F. 1977, A&A, 57, 285
Elgarøy, Ø. 1961, Astrophysica Norvegica, 7, 123
Fleishman, G., & Arzner, K. 2000, A&A, 358, 776
Fleishman, G. D., Gary, D. E., & Nita, G. M. 2003, ApJ, 593, 571
Fleishman, G. D., & Mel'nikov, V. F. 1998, Physics Uspekhi, 41, 1157
Fleishman, G. D., & Melnikov, V. F. 1999, in ESA Special Publication, 9, Magnetic Fields and Solar Processes, eds. A. Wilson et al., 1247
Fleishman, G. D., & Yastrebov, S. G. 1994, Sol. Phys., 154, 361
Fu, Q., Qin, Z., Ji, H., & Pei, L. 1995, Sol. Phys., 160, 97

Fu, Q., Ji, H., Qin, Z., et al. 2004, Sol. Phys., 222, 167
Guedel, M., & Benz, A. O. 1990, A&A, 231, 202
Guo, Y., Ding, M. D., Wiegelmann, T., & Li, H. 2008, ApJ, 679, 1629
Jing, J., Chae, J., & Wang, H. 2008, ApJL, 672, L73
Kosovichev, A. G., & Sekii, T. 2007, ApJL, 670, L147
Kuijpers, J., van der Post, P., & Slottje, C. 1981, A&A, 103, 331
Li, C., Dai, Y., Vial, J. C., et al. 2009, A&A, 503, 1013
Lin, J., & Forbes, T. G. 2000, J. Geophys. Res., 105, 2375
Melrose, D. B., & Dulk, G. A. 1982, ApJ, 259, 844
Messmer, P., & Benz, A. O. 2000, A&A, 354, 287
Minoshima, T., Imada, S., Morimoto, T., et al. 2009, ApJ, 697, 843
Ning, Z. 2008, Sol. Phys., 247, 53
Rozhansky, I. V., Fleishman, G. D., & Huang, G. L. 2008, ApJ, 681, 1688
Sharma, R. R., & Vlahos, L. 1984, ApJ, 280, 405
Shibata, K., Masuda, S., Shimojo, M., et al. 1995, ApJL, 451, L83
Sirenko, E. A., & Fleishman, G. D. 2009, Astronomy Reports, 53, 369
Slottje, C. 1978, Nature, 275, 520
Staehli, M., & Magun, A. 1986, Sol. Phys., 104, 117
Tajima, T., Benz, A. O., Thaker, M., & Leboeuf, J. N. 1990, ApJ, 353, 666
Tan, B. 2008, Sol. Phys., 253, 117
Tan, B. 2010, Ap&SS, 325, 251
Tan, B. 2013, ApJ, 773, 165
Tan, B., Chen, N., Yang, Y.-H., et al. 2019, ApJ, 885, 90
Tan, B.-L., Yan, Y., Li, T., Zhang, Y., & Chen, X.-Y. 2020, RAA (Research in Astronomy and Astrophysics), 20, 090
Tan, B., & Tan, C. 2012, ApJ, 749, 28
Tan, B., Yan, Y., Tan, C., & Liu, Y. 2007, ApJ, 671, 964
Tan, B., Zhang, Y., Tan, C., & Liu, Y. 2010, ApJ, 723, 25
Tanaka, H., Castelli, J. P., Covington, A. E., et al. 1973, Sol. Phys., 29, 243
Wang, S. J., Yan, Y. H., Liu, Y. Y., et al. 2008, Sol. Phys., 253, 133
Wentzel, D. G. 1991, ApJ, 373, 285
Winglee, R. M., Dulk, G. A., & Pritchett, P. L. 1988, ApJ, 328, 809
Yan, Y., Tan, C., Xu, L., et al. 2002, Science in China A: Mathematics, 45, 89
Yan, Y., Zhang, J., Wang, W., et al. 2009, Earth Moon and Planets, 104, 97
Zhang, J., Li, L., & Song, Q. 2007, ApJL, 662, L35
Zhang, Y., Tan, B., & Yan, Y. 2008, ApJL, 682, L133